

Received September 1, 2020, accepted September 14, 2020, date of publication September 18, 2020, date of current version September 30, 2020.

Digital Object Identifier 10.1109/ACCESS.2020.3024977

Terramechanics Modeling and Grouser Optimization for Multistage Adaptive Lateral Deformation Tracked Robot

YIDONG BAI¹, LINGYU SUN, (Member, IEEE), AND MINGLU ZHANG, (Member, IEEE)

School of Mechanical Engineering, Hebei University of Technology, Tianjin 300401, China

Corresponding author: Lingyu Sun (sunlyu78@126.com)

This work was supported in part by the National Natural Science Foundation of China under Grant 61733001 and Grant U1913211, in part by the Hebei Province Key Basic Research in Applied Basic Research Program under Grant 17961820D, and in part by the Hebei Province Innovation Funding Project for Graduate Students under Grant CXZZBS2020030.

ABSTRACT A multistage adaptive lateral deformation tracked robot was designed to improve the passing ability of field robots. The designed robot can change its width under the combined action of space barrier constraint and internal stored elastic potential energy. The lateral sliding friction affected by grouser parameters during lateral deformation is a key factor that determines whether or not the robot can achieve deformation. This study focuses on the track terramechanics and grouser parameter optimization. On the basis of the theory of terramechanics, the interaction of the flexible track lateral movement with the ground model and traction model was established. Taking the requirement of traction as the constraint condition and the minimum lateral sliding resistance as the optimization objective, we used the multitarget optimization algorithm (NSGA-II) to optimize and analyze the grouser parameters. Then, the optimal combination of grouser parameters was obtained. Simulation analysis was carried out on RecurDyn software to complete the simulation verification of the lateral force and traction force under different grouser parameters. The correctness of the theoretical model and the optimization of the grouser parameters was verified through prototype experiments.

INDEX TERMS Multistage deformation, tracked robot, track lateral movement, grouser parameter optimization, RecurDyn simulation.

I. INTRODUCTION

Natural disasters and accidents have occurred frequently in recent years, and the corresponding loss of lives and properties has been increasing. When a mobile robot encounters an environment that requires it to pass through a narrow space, such as a narrow passage, a ruin passage, and a narrow mine tunnel, it usually uses a method to bypass such an environment. The use of such method increases the robot's moving distance, execution time, and energy consumption, thereby rendering it useless in certain tasks involving a narrow environment. The use of intelligent mobile robots to perform emergency rescue, daily inspection, monitoring, and early warning in complex and dangerous environments has thus become increasingly important, and related research has achieved positive results.

The associate editor coordinating the review of this manuscript and approving it for publication was Bilal Alatas¹.

Numerous countries have developed a variety of mobile robots for reconnaissance and rescue to ensure the safety and efficiency of these tasks. The moving mechanisms used include snake, wheeled, tracked, foot, wheel-tracked composite, wheel-leg composite, and so on [1]–[5]. Tracked robots are widely used because tracked structures can adapt to complex ground environments. Fixed tracked robots include Packbot, Quince, Dragon Runner, etc. [6]–[8]; deformable tracked robots include TSSTV, AMOEBA-I, RESCUER, etc. [9], [10]. Although current reconnaissance and rescue robots have their own characteristics, they cannot enter spaces that are smaller than their own widths due to their mechanical structure, dimensions, driving force, and other factors. Moreover, they cannot complete rescue tasks well in complex disaster environments [11].

To understand the trafficability of tracked robots in different terrains and improve their adaptability in complex environments, previous research has explored the mechanism

of the interaction between tracked structures and the ground on the basis of the theory of terramechanics [12]. The related methods are classified into four categories, namely, empirical, semi-empirical, physics-based, and numerical analysis methods [13]–[16]. The current research mainly analyzes the influence of ground physical parameters on the traction ability of vehicles by establishing a terramechanics model and focuses on the modeling of large-scale tracked vehicles. However, the analyses of small tracked robots, especially tracked robots made of flexible rubber, are relative few.

On the basis of the research progress described herein, we identify two major deficiencies of current field robots that need to be resolved to facilitate their use in complex operating environments:

- Using the constraints of the environment to deform robots effectively and eliminating the dependence on active driving to generate energy consumption caused by robot deformation so as to enable robots to operate for long periods and in wide working spaces;
- Solving the effect of the grouser on the lateral sliding force and traction. The robot is subjected to lateral sliding force when it turning and moving laterally, and the smaller the lateral sliding force, the better for the robot. At the same time, lateral sliding force and traction show a nonlinear relationship, that is, they are coupled, and they influence each other. Optimizing the grouser to minimize the lateral sliding resistance under the condition in which the traction force is large enough.

To address these deficiencies, especially the former one that has emerged as a hot research topic, we designed a multi-stage adaptive lateral deformation tracked robot, established a tracked terramechanics model made of flexible rubber, optimized track parameters, and completed simulation and experimental verification. The main contributions of this work are summarized as follows:

- A robot is designed under the combined action of space obstacle constraints and internally stored elastic potential energy. The proposed robot can deform perpendicularly toward the direction of movement and change its own width to enter a narrow space;
- The terramechanics model of a small tracked robot made of flexible rubber is established, and the track parameters are optimized;
- A simulation analysis is completed using RecurDyn software, and the experimental verification of the prototype is carried out on field sand.

This article is organized as follows. Section II introduces the structure and deformation process of the robot. Section III discusses the theory of terramechanics and provides in detail the effects of grouser parameters. The lateral sliding model and traction model of the flexible tracked robot are also described in this section. Section IV presents the optimization of the grouser parameters based on the established models. Sections V and VI respectively describe the simulation and outdoor verification processes. The simulation

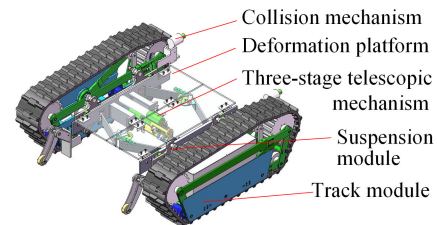


FIGURE 1. Structural diagram of the robot.

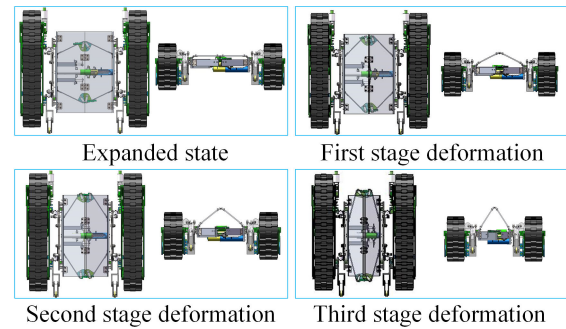


FIGURE 2. Three-level deformation process.

and experimental results are also extensively explained. Section VII presents the conclusions.

II. ROBOT STRUCTURE DESIGN AND ANALYSIS

The structure of the robot designed in this work is shown in Fig. 1. Following a modular design, we adopt the modular mechanical connection scheme of a “building block” in our robot design. The robot is composed of two track modules, two suspension modules, two collision mechanism modules, and a deformation platform module. The three-stage telescopic mechanism is included by deformation platform module. The modules are connected by a universal lock and can be disassembled quickly and carried conveniently.

For small robots, it has the advantages of large load, long driving distance, and strong ability to overcome obstacles. For robots with the same size, it can deform transversely to change its width and thus exhibits strong terrain passability and environmental adaptability.

In addition, the width of the tracked robot has an important impact on turning stability and energy consumption. With the increase of width, the stability of turning is better, the energy consumption of turning is smaller, and less likely to rollover. However, when the width of the robot is too large, it cannot pass through some narrow spaces, so the working range is limited.

The multistage deformation process of the robot is shown in Fig. 2. This process is realized by the collision mechanism in front of the robot and the deformation platform mechanism in the middle. The internal core structure of the deformation platform is a three-stage step-by-step telescopic mechanism, which comprises three tension springs. After the collision mechanism comes into contact with obstacles, the limit device of the telescopic mechanism is triggered,

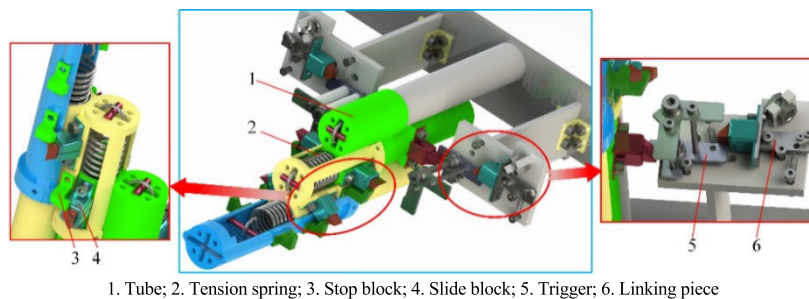


FIGURE 3. Three-stage telescopic structure.

and the first-stage tension spring is released to pull the two tracks to move to the middle. At the same time, the platform deforms upward, and the robot completes the first-stage lateral deformation. If the robot is still unable to pass through the narrow space, the collision mechanism collides with the obstacle again, and the secondary tension spring is released to complete the second lateral deformation. After three collisions, the deformation degree of the robot reaches the maximum, and the deformation process is realized step by step.

The three-stage telescopic mechanism is the main mechanism for the robot to achieve deformation, and the structure, which include four spring tubes, three extension springs, two reset springs, and the corresponding limit device, is shown in Figure 3.

When the platform is undeformed, three extension springs are in a stretched state. The sliding block is pressed against the fixed block to limit the contraction of the spring. After the collision mechanism installed on the track module collides with the external objects, the collision mechanism pulls the linking piece, which drives the trigger to rotate and removes the restriction on the slide block. The extension spring is contracted back while the linking piece and the trigger are restored to the initial position under the extension of the return spring, and the first deform is completed. After the second and third collisions using the same steps, the second and third deformation processes are completed.

During the lateral deformation of the robot, the two tracks move to the middle through friction with the ground. Therefore, an important factor influencing the capability of the robot to smoothly achieve deformation is the magnitude of friction during translation. The size of the lateral sliding friction also exerts a significant impact on spring selection, structural analysis, and optimization design.

Among the many factors that affect the lateral sliding friction, the grouser parameter is the important factor that must be considered. During the contact between the grouser and the ground, parameters such as height, thickness, and pitch produce different friction forces. Moreover, different tractions are produced during the driving process. Most existing research focused on the rolling friction of the track and the influence of track structure parameters on traction, and thus, little is known about the friction of the lateral

translation of the track [17], [18]. Therefore, following the theory of terramechanics, we model the interaction between the flexible track and the ground. Two factors, namely, lateral sliding friction and traction, are considered to optimize the grouser parameters. Simulation and experimental verification are then performed.

III. TRACK-GROUND INTERACTION MODEL

The research on the contact between the track and the ground belongs to the category of vehicle terramechanics. Researchers have carried out in-depth investigations, and they have established numerous theories, such as the vehicle cone index and Bekker theory [19]–[21]. With this research foundation, the study on the optimization of grouser parameters is carried out.

Herein, the robot adopts a flexible rubber track, which causes great deformation during movement. The grouser effect is also prominent during the lateral sliding process. The grouser effect is mainly reflected in the shear force of the grouser on the soil, and the coupling effect of track subsidence and lateral slip is analyzed [22], [23]. On the basis of the theory of vehicle terramechanics, we consider the impact of the grouser effect and establish the lateral sliding model and traction model of the flexible track. Then, considering the shape parameters of the grouser, we analyze a single grouser in terms of lateral sliding and traction force. With the subsidence distribution function, we finally establish the lateral sliding force model and traction force model of the whole track.

A. SUBSIDENCE DISTRIBUTION FUNCTION

The distribution of subsidence is related not only to soil type but also to the geometric structure of the track and ground [24]. Therefore, on the basis of the characteristics of the flexible track, a function suitable for the calculation of the subsidence distribution of the flexible track is established.

The interaction model between the whole robot and the ground is shown in Fig. 4. The deformation of the track leads to a curve in the middle of the contact with the soil. In addition, when the robot moves, the soil heaves at the front part of the first bearing wheel. Therefore, the calculation of subsidence is divided into three parts: the first load-bearing part, the middle track part, and the other three load-bearing

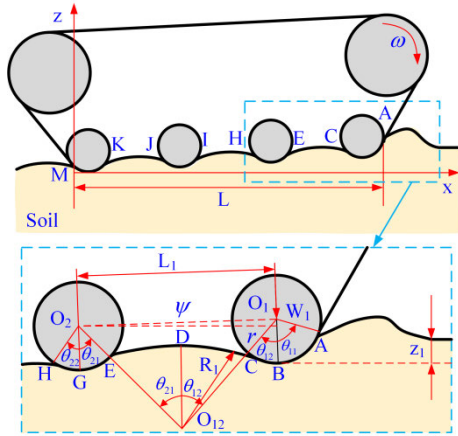


FIGURE 4. Whole track on deformable terrain.

parts; the three parts maintain the continuity of the track shape and thus ensure the continuity of track subsidence distribution.

The sinkage of the bearing wheel is z_i and can be obtained from the empirical formula [25]

$$\begin{cases} z_1 = \left[3W_1 / \left[(3-n) (k_c + bk_\phi \sqrt{2r}) \right] \right]^{2/(2n+1)} \\ z_i = z_{i-1} + L_1 \sin \psi \quad (i = 2, 3, 4) \end{cases} \quad (1)$$

where W_1 is the radial vertical load on the bearing wheel, n is the sinkage exponent of soil, k_c is the cohesion of soil, k_ϕ is the frictional modulus of soil, r is the radius of the bearing wheel, L_1 is the distance of the bearing wheel, and ψ is the horizontal angle.

The entry angle of the road wheel and soil is θ_{i1} , and the departure angle is θ_{i2} according to the geometric relations and experience [26]:

$$\begin{cases} \theta_{11} = \cos^{-1} (1 - z_1/r) \\ \theta_{i1} = \arcsin \frac{L_1}{2(r + R_{i-1})} \quad (i = 2, 3, 4) \\ \theta_{i2} = 0.6\theta_{i1} \quad (i = 1, 2, 3, 4) \end{cases} \quad (2)$$

As the deformation of the track is regular under the condition of soft road, we assume that the part of the crawler in contract with the ground is arc-shaped with a radius of R_i ,

$$R_i = \frac{L_1}{2 \sin (\theta_{i2} + \psi)} - r \quad (i = 1, 2, 3). \quad (3)$$

In summary, the subsidence of any point under the wheel is as follows:

$$z = z_i - r(1 - \cos \theta) \quad (i = 1, 2, 3, 4), \quad (4)$$

The subsidence of any point under the middle track is as follows:

$$z = z_i - r(1 - \cos \theta_{i+1,1}) - R_i (\cos \theta - \cos \theta_{i2}) \quad (i = 1, 2, 3). \quad (5)$$

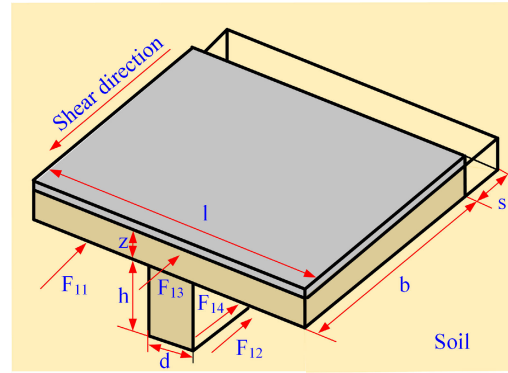


FIGURE 5. Single track shoe load force.

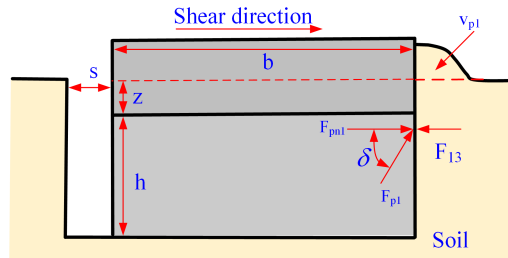


FIGURE 6. Track traverse scraping model.

B. TRACK LATERAL SLIDING MODEL

By analyzing the literature, we know that the “in-line” track is often used in small robots, which are suitable for various complex environments, such as obstacle crossing and stair descent. Therefore, the grouser shape studied in this work is “in line”. The force analysis of a single track shoe is shown in Fig. 5. F_{11} is the bottom force of the track shoe, F_{12} is the bottom force of the grouser, F_{13} is the force perpendicular to the side of the track shoe and grouser, F_{14} is the force at both ends of the grouser, d is the grouser thickness, h is the grouser height, l is the grouser pitch, b is the track width, and s is the sliding distance.

The stresses at the bottom of the track shoe and grouser are p_1 and p_2 , respectively.

$$\begin{cases} p_1 = \left(\frac{k_c}{b} + k_\phi \right) z^n \\ p_2 = \left(\frac{k_c}{b} + k_\phi \right) (z + h)^n \end{cases} \quad (6)$$

$$F_{11} = b(l - d) \eta(v) (c + p_1 \tan \varphi), \quad (7)$$

$$F_{12} = bd \eta(v) (c + p_2 \tan \varphi), \quad (8)$$

$$\eta(v) = \frac{\eta_{\max} v + 0.12}{v + 0.12}, \quad (9)$$

where c is the cohesion of soil, φ is the internal friction angle of soil, v is the shear rate, and η is the amplification factor.

During the lateral movement of the track, a part of the soil is scraped up, as shown in Fig. 6, where V_{p1} is the volume of the soil scraped. According to the theory of retaining wall, the soil close to the track is squeezed, and the soil is in

Rankine stress state. F_{pn1} is the force acting vertically on the track, and F_{p1} is the shear force of the soil on the grouser.

$$v_{p1} = (hd + zl)s, \quad (10)$$

$$F_{pn1} = d \int_0^h (\gamma z K_{p\gamma} + \gamma v_{p1} K_{pq} + c K_{pc}) dz + l \int_0^z (\gamma z K_{p\gamma} + \gamma v_{p1} K_{pq} + c K_{pc}) dz, \quad (11)$$

$$F_{p1} = c(hd + lz) + F_{pn1} \tan \delta, \quad (12)$$

$$F_{13} = F_{pn1} + F_{p1}, \quad (13)$$

$$F_{14} = \frac{phb}{\pi} \arctan \frac{h}{l}, \quad (14)$$

where γ is the unit weight of soil; $K_{p\gamma}$, K_{pq} , K_{pc} are the coefficients related to soil strength; δ is the friction angle of the soil and track; and p is the average ground pressure.

In summary, the maximum force on each track shoe under lateral sliding is as follows:

$$F_{Ll} = F_{11} + F_{12} + F_{13} + F_{14}, \quad (15)$$

The maximum force on the whole track is as follows:

$$F_L = \sum_{l=1}^N F_{Ll}, \quad (16)$$

where F_{Ll} is the lateral force on the l track shoe and N is the number of track shoes in contact with the ground.

C. TRACK TRACTION MODEL

Traction is an important index to evaluate vehicle performance, and it is given by the difference between track adhesion and driving resistance. Driving resistance includes compaction resistance and bulldozing resistance. The adhesion and driving resistance of a single track shoe are analyzed, the maximum adhesion model of the whole track is then established, and the maximum traction model of the whole track is obtained.

1) TRACK ADHESION MODEL

The adhesion model of a single track shoe is shown in Fig. 7. F_{21} is the horizontal force acting on the bottom of the track shoe, F_{22} is the horizontal force acting on the bottom of the grouser, F_{23} is the force acting on the vertical surface of the grouser, and F_{24} is the horizontal force acting on the end of the track shoe. j is the sliding distance, K is the shearing deformation modulus of soil, and i is the slip rate.

$$j = ix, \quad (17)$$

$$F_{21} = b(l - d)\eta(v)[c + p_1 \tan \varphi], \quad (18)$$

$$F_{22} = bd\eta(v)[c + p_2 \tan \varphi], \quad (19)$$

$$v_{p2} = (h + z)bj, \quad (20)$$

$$F_{pn2} = b \left[\int_0^h (\gamma z K_{p\gamma} + \gamma v_{p2} K_{pq} + c K_{pc}) dz + \int_0^z (\gamma z K_{p\gamma} + \gamma v_{p2} K_{pq} + c K_{pc}) dz \right] (1 - e^{-j/K}), \quad (21)$$

$$F_{p2} = cb(h + z) + F_{pn2} \tan \delta, \quad (22)$$

$$F_{23} = F_{pn2} + F_{p2}, \quad (23)$$

$$F_{24} = \frac{phl}{\pi} \arctan \frac{h}{b}. \quad (24)$$

In summary, the maximum adhesion of each track shoe is as follows:

$$F_{Tl} = F_{21} + F_{22} + F_{23} + F_{24}. \quad (25)$$

The maximum adhesion of the whole track is as follows:

$$F_T = \sum_{l=1}^N F_{Tl}. \quad (26)$$

where F_{Tl} is the adhesion force on the l track shoe.

2) DRIVING RESISTANCE

a: COMPACTION RESISTANCE

The stress at the bottom of the track meets the requirements as follows:

$$p_1 bL \left(1 - \frac{d}{l}\right) + p_2 bL \frac{d}{l} = \frac{W}{2}, \quad (27)$$

The work done by the robot at distance S is as follows:

$$E_1 = 2bS \left(1 - \frac{d}{l}\right) \int_0^{z_0} p_1 dz + 2bS \frac{d}{l} \int_0^{z_0} p_2 dz, \quad (28)$$

$$E_1 = F_{RC} S, \quad (29)$$

where F_{RC} is the compaction resistance.

Organizing the formula for compaction resistance yields

$$F_{RC} = 2 \frac{k_c + bk_\varphi}{n + 1} \left\{ \left[z_0^{n+1} \left(1 - \frac{d}{l}\right) \right] + \frac{d}{l} (z_0 + h)^{n+1} \right\}. \quad (30)$$

b: BULLDOZING RESISTANCE

According to the theory of retaining wall, bulldozing resistance F_{RT} is obtained as

$$F_{RT} = 2b \left(cz_0 K_{p\gamma} + 0.5 z_0^2 \gamma K_{p\gamma} \right). \quad (31)$$

In summary, the maximum traction F_H of the whole track is

$$F_H = F_T - F_{RC} - F_{RT}. \quad (32)$$

IV. GROUSER PARAMETER OPTIMIZATION

The force process of the adaptive deformation movement is mainly concentrated on the lateral sliding force of a track shoe. The interaction between the lateral sliding of the track and the soil is an important factor that determines whether a robot can achieve deformation successfully. Therefore, on the basis of the lateral sliding force model and traction model established herein, the grouser parameters are optimized, and the influence of each parameter is analyzed.

Lateral sliding force and traction show a nonlinear relationship, that is, they are coupled, and they influence each other. When optimizing the design of the grouser to reduce the lateral force, the traction force must also be considered because the reduction of the lateral force may mean that the traction force is also reduced. Therefore, our optimization

TABLE 1. Calculation of model parameters.

Parameter	Unit	Value
w_l	kN	0.04
r	m	0.03
L_l	m	0.14
s	m	0.06
v	m/s	0.1
η	$/$	1.41
γ	kN/m^3	17
δ	$(^\circ)$	30
p	kPa	6.86
n	$/$	0.5
kc	kN/m^{n+1}	13.19
k_ϕ	kN/m^{n+2}	692.15
c	kPa	4.14
ϕ	$(^\circ)$	13

TABLE 2. Selection range of grouser parameters.

Grouser parameter	Lower limit	Upper limit
Height (h)	0	20 mm
Thickness (d)	1 mm	10 mm
Pitch (l)	20 mm	40 mm

goal is to minimize the lateral sliding resistance under the condition in which the traction force is large enough.

On the basis of the proposed lateral sliding force model and traction model and by meeting the requirements of traction force as the constraint condition and reducing the lateral sliding resistance as the optimization objective, the optimization mathematical model is established as follows:

$$\begin{cases} \min F_L = \sum_{l=1}^N F_{Ll} \\ s.t. F_H \geq F_S \end{cases} \quad (33)$$

where F_S is the minimum traction to meet the performance requirements of the robot.

The optimization design of the grouser is a multidimensional and complex problem; thus, the multitarget optimization algorithm (NSGA-II) is used to optimize and analyze the grouser parameters. Field tracked robots often works under the clayey soil environment, so clayey soil is selected to optimize grouser parameters. The calculation parameters for clayey soil are shown in Table 1 [27], [28].

The ranges of the grouser parameters variables that meet actual design constraints, strengths, and other requirements are shown in Table 2.

In the MATLAB programming simulation environment, the optimal result is obtained after iterative optimization. When the grouser height, thickness, and pitch are 8, 5, and 22 mm, respectively, the traction force is 389 N, and the lateral sliding friction force is 203 N. According to the proposed lateral force and traction models, the lateral force and traction are plotted with the changes in grouser parameters (Fig. 8). The results show that when the grouser parameters are the same as the optimization results, the lateral force reaches the

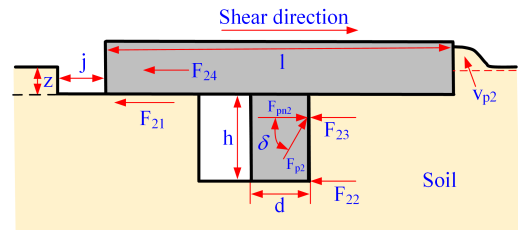


FIGURE 7. Track adhesion model.

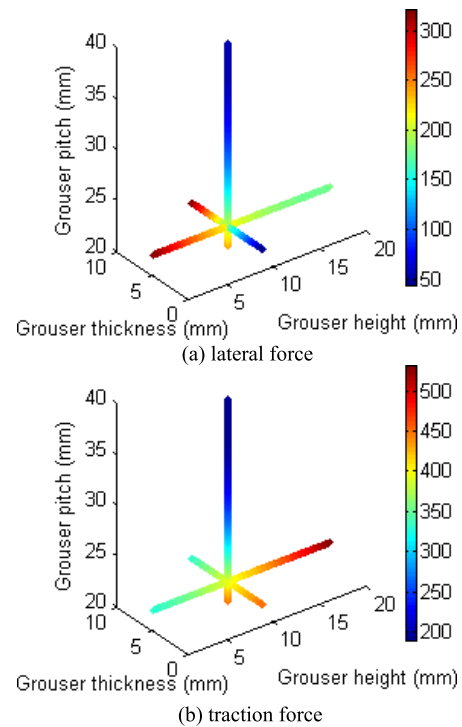


FIGURE 8. Change diagram of lateral and traction forces.

minimum while the traction force reaches the maximum; this outcome is consistent with the optimization result.

V. LATERAL FORCE AND TRACTION SIMULATION

The grouser parameters are optimized on the clayey soil in section IV. To verify the theoretical model and optimization results of the grouser parameters, the simulation and experimental verification are completed on the clayey soil in sections V and VI respectively. In addition, to compare with the results on the clayey soil, simulation and experiment are carried out on the sandy loam.

Simulation model is established that is based on the RecurDyn multibody system dynamics simulation software. The model is used to calculate the lateral forces and tractions of different grouser parameters. RecurDyn comprises a low-mobility track system toolkit Track (LM) that is designed specifically for tracked vehicles and can conveniently model tracks, drive wheels, and other components.

A three-dimensional model of the platform is built in SolidWorks software and imported into RecurDyn/Track (LM). Components such as crawlers, tensioning wheels, driving

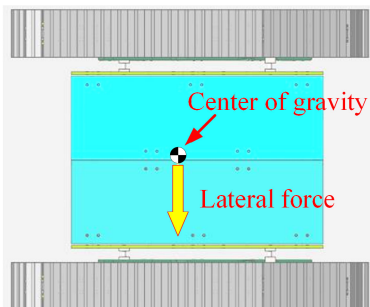


FIGURE 9. Lateral force measurement model.

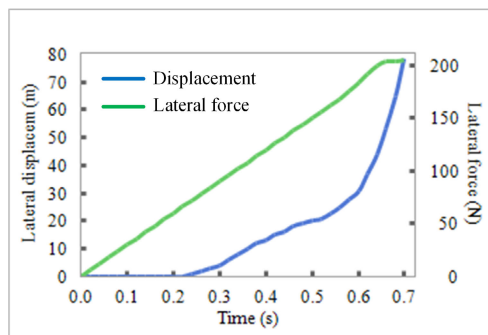


FIGURE 10. Lateral force-lateral displacement curve.

wheels, etc. are parameterized in Track (LM). The whole system is then assembled, and the multibody dynamic model is established. On the basis of the established multibody dynamic model, the lateral force and traction of the robot are verified.

A. LATERAL FORCE SIMULATION TEST

To test the pulling force required for the lateral movement of the robot, we add a gradually increasing lateral force at the center of gravity of the model and perpendicular to the direction of robot movement (Fig. 9). The simulation results are shown in Fig. 10. When the pulling force is less than the maximum static friction force experienced by the robot, the robot is at a standstill. As the pulling force gradually increases and the pulling force exceeds the maximum static friction force received by the robot, the robot starts to move laterally; the lateral force is measured at this time. The average value is calculated through multiple simulations, and the lateral force is obtained.

B. TRACTION SIMULATION TEST

To test the traction of the robot, we add a driving force that should make the robot move forward at a constant speed. When the robot movement state is stable, a gradually increasing pulling force at the center of gravity and opposite to the movement direction is added (Fig. 11). As the pulling force increases, the speed decreases gradually and drops to zero, in which case the robot is in a slipping state. At this time, the maximum traction is obtained. The simulation results are shown in Fig. 12. The average value is calculated through multiple simulations, and the traction is obtained.

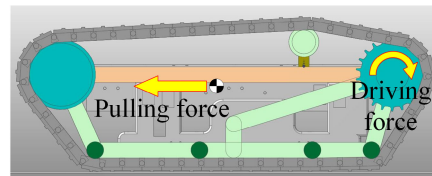


FIGURE 11. Traction force measurement model.

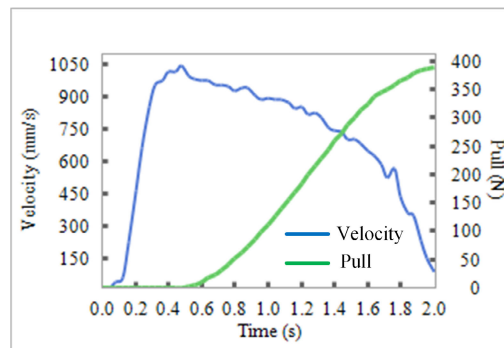


FIGURE 12. Speed-slip rate curve.

To verify the correctness of the theoretical analysis and simulation model, we take four values of grouser height, thickness, and pitch and simulate them with a control variable method. The results and errors are shown in Table 3 and Table 4. The results of the lateral sliding force model and traction model, as well as the results in Table 3 and Table 4, are plotted in Fig. 13. The table and graph show that the theoretical analysis and computer simulation value share the same trend. On the clayey soil, the maximum absolute error is 14 N, the average is 7.3 N, the maximum relative error is 12.77%, and the average is 3.6%. On the sandy loam, the maximum absolute error is 18 N, the average is 7.2 N, the maximum relative error is 11.11%, and the average is 3.3%. Although certain differences exist, they are all within the acceptable range. Thus, the validity of the models is verified.

VI. EXPERIMENTAL VERIFICATION

On the basis of the theoretical and simulation results, the prototype of the robot is developed, and an outdoor experiment is carried out. According to the calculation results, the height, thickness, and pitch of the grouser are taken as 8, 5, and 22 mm, respectively.

A. EXPERIMENT PROCEDURE

The experimental scene is shown in Fig. 14. The experimental method is the same as that in the simulation model, and the experiment is completed on outdoor. A high-precision digital display force dynamometer is adopted, and the measurement accuracy is 0.01 N. The supporting data analysis software of the dynamometer can display, record, and store measurement data in real time. The specific experimental process is as follows:

Lateral force test process: The robot is placed on the flat soil, and the projection point of the robot’s center of gravity

TABLE 3. Comparison of simulated and calculated values on the clayey soil.

Grouser height (mm)	Grouser thickness (mm)	Grouser pitch (mm)	Lateral simulate (N)	Lateral calculate (N)	Absolute error (N)	Relative error (%)	Traction simulate (N)	Traction calculate (N)	Absolute error (N)	Relative error (%)
2			312	305	7	2.24	348	341	7	2.01
6	5	22	260	255	5	1.92	360	348	12	3.33
8			215	209	6	2.79	400	395	5	1.25
16	1	22	193	182	11	5.70	496	487	9	1.81
			98	90	8	8.16	456	436	14	1.75
8	3	22	154	150	4	2.60	445	440	5	3.15
	5		215	209	6	2.79	400	395	5	1.25
	10		340	331	9	2.65	352	343	6	2.56
8	5	22	215	209	6	2.79	400	395	5	1.25
		30	118	117	1	0.85	262	253	6	3.44
		35	81	72	9	11.11	221	214	7	3.17
		40	63	57	6	9.52	211	207	4	1.90

TABLE 4. Comparison of simulated and calculated values on the sandy loam.

Grouser height (mm)	Grouser thickness (mm)	Grouser pitch (mm)	Lateral simulate (N)	Lateral calculate (N)	Absolute error (N)	Relative error (%)	Traction simulate (N)	Traction calculate (N)	Absolute error (N)	Relative error (%)
2			302	299	3	0.99	342	336	6	1.75
6	5	22	252	249	3	1.19	354	366	12	3.39
8			210	203	7	3.33	396	389	7	1.77
16	1	22	185	176	9	4.86	489	475	14	2.86
			79	71	8	10.13	445	438	7	1.57
8	3	22	128	127	1	0.78	422	414	8	1.90
	5		210	203	7	3.33	396	389	7	1.77
	10		334	321	13	3.89	338	330	8	2.37
8	5	22	210	203	7	3.33	396	389	7	1.77
		30	92	95	3	3.26	246	240	6	2.44
		35	65	61	4	6.15	214	196	18	8.41
		40	47	53	6	12.77	198	193	5	2.53

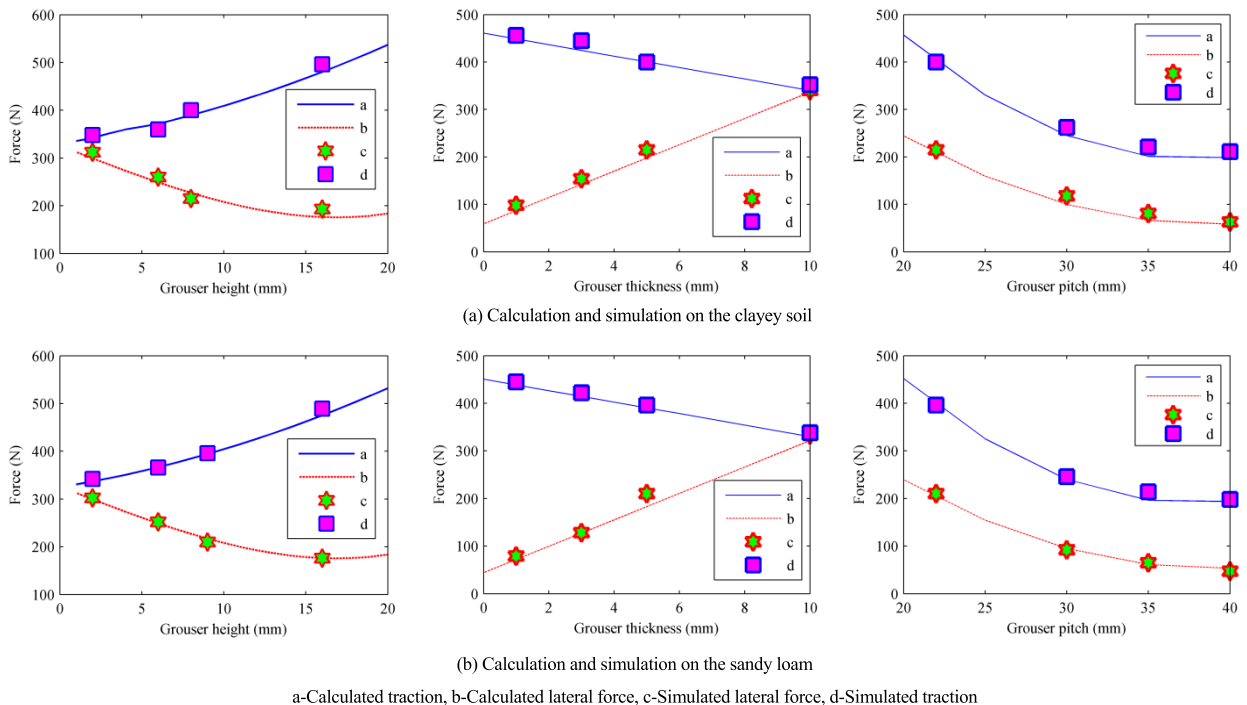


FIGURE 13. Influence of grouser parameters on lateral force and traction on the sandy loam and clayey soil.



FIGURE 14. Prototype robot and experiment.

is pulled on the side with a dynamometer. As the pulling force gradually increases, the robot starts to move laterally. The measurement is completed when the robot moves at a constant speed. The effective value is taken, and the average value is calculated to obtain the lateral force measured at this time. After multiple measurements, the average value of each lateral force is calculated to obtain the final lateral force.

Traction test process: The robot is driven forward at a constant speed on flat soil, and the projection point of the robot’s center of gravity is pulled from behind with a dynamometer. As the pulling force gradually increases, the robot starts to slip until the slip rate reaches 100%. The forward speed then drops to zero, and the measurement is completed. After multiple measurements, the average value of each traction force is calculated to obtain the final traction force.

B. EXPERIMENTAL RESULTS AND ANALYSIS

The simulated and experimental values are listed in Table 5 and Table 6. Each lateral force and traction experiment is measured in 10 groups on the clayey soil and sandy loam. On the clayey soil, the average of the lateral sliding friction force is 219 N, and the average of maximum traction is 391 N. The variances of the lateral force and traction obtained in the experiment are 2.19 and 3.35, respectively. On the sandy loam, the average of the lateral sliding friction force is 211 N, and the average of maximum traction is 382 N. The variances of the lateral force and traction obtained in the experiment are 3.27 and 2.56, respectively. These values indicate that the experimental data are concentrated, the fluctuation is small, the result is stable, and the experimental program is accurate and effective.

Comparing the simulation value and experimental value shows that the maximum absolute error is 9 N and that the maximum relative error is 3.8%. The experimental value is close to the theoretical value, and the error is small. This outcome verifies the correctness and feasibility of the built lateral

TABLE 5. Comparison of experimental results on the clayey soil.

	Experiment. mean	Experiment. variance	Simulated mean	Absolute error	Relative error
Lateral force	219 N	2.19	215 N	4 N	1.8%
Traction	391 N	3.35	400 N	9 N	2.3%

TABLE 6. Comparison of experimental results on the sandy loam.

	Experiment. mean	Experiment. variance	Simulated mean	Absolute error	Relative error
Lateral force	211 N	3.27	203 N	8 N	3.8%
Traction	382 N	2.56	389 N	7 N	1.8%

slip model and traction model, as well as the correctness of the optimization results of the grouser parameters.

VII. CONCLUSION AND FUTURE WORK

A. SUMMARY OF CONCLUSIONS

To meet the requirements of high mobility and high trafficability of field robots, we design a multistage adaptive lateral deformation tracked robot and optimize the grouser parameters. The following achievements and conclusions are obtained.

First, the designed robot can change its width through lateral deformation. The design solves the common outstanding problems of existing field operation robots. The designed has relatively strong terrain passability and environmental adaptability, and it can complete field tasks efficiently and safely.

Second, the lateral sliding model and traction model of the whole track are established, along with the grouser parameters. The multitarget optimization algorithm (NSGA-II) is used to optimize and analyze the grouser parameters. The minimum lateral sliding force is 215 N when the height, thickness, and pitch are 8, 5, and 22 mm, respectively, under the condition of meeting the traction requirements.

Third, the simulation model is built in RecurDyn/Track (LM), the robot prototype is developed, and the experimental verification is completed on outdoor. The results obtained are close to the theoretical values, and the correctness of the theoretical model and simulation results is verified.

B. FUTURE WORK

After the robot completes its deformation, it cannot return to its original width with its own force. Therefore, we will improve the deformation platform and add a driving mechanism on the platform to assist the robot in completing the deployment deformation.

In terms of grouser parameter optimization, we only completed the modeling and verification on the clayey soil and the sandy loam. In the next step, we will perform analyses and experiments on clay road, gravel road, and grassland.

REFERENCES

[1] J. Gao, X. Gao, W. Zhu, J. Zhu, and B. Wei, “Design and research of a new structure rescue snake robot with all body drive system,” in *Proc. IEEE Int. Conf. Mechatronics Autom.*, Aug. 2008, pp. 119–124, doi: 10.1109/ICMA.2008.4798737.

- [2] F. Xu, X. Liu, W. Chen, and C. Zhou, "Dynamic switch control of steering modes for four wheel independent steering rescue vehicle," *IEEE Access*, vol. 7, pp. 135595–135605, 2019, doi: [10.1109/ACCESS.2019.2941914](https://doi.org/10.1109/ACCESS.2019.2941914).
- [3] M. Raibert, K. Blankespoor, G. Nelson, and R. Playter, "BigDog, the rough-terrain quadruped robot," *IFAC Proc. Volumes*, vol. 41, no. 2, pp. 10822–10825, 2008, doi: [10.3182/20080706-5-kr-1001.01833](https://doi.org/10.3182/20080706-5-kr-1001.01833).
- [4] P. Ben-Tzvi and W. Saab, "A hybrid tracked-wheeled multi-directional mobile robot," *J. Mech. Robot.*, vol. 11, no. 4, pp. 1–10, Aug. 2019, doi: [10.1115/1.4043599](https://doi.org/10.1115/1.4043599).
- [5] L. Bai, J. Guan, X. Chen, J. Hou, and W. Duan, "An optional passive/active transformable wheel-legged mobility concept for search and rescue robots," *Robot. Auto. Syst.*, vol. 107, pp. 145–155, Sep. 2018.
- [6] K. Michael and M. G. Michael, "The packbots are coming: Boosting security at the 2014 FIFA world cup," *IEEE Consum. Electron. Mag.*, vol. 3, no. 3, pp. 59–61, Jul. 2014, doi: [10.1109/MCE.2014.2317914](https://doi.org/10.1109/MCE.2014.2317914).
- [7] K. Nagatani, S. Kiribayashi, Y. Okada, K. Otake, K. Yoshida, S. Tadokoro, T. Nishimura, T. Yoshida, E. Koyanagi, M. Fukushima, and S. Kawatsuma, "Emergency response to the nuclear accident at the fukushima daiichi nuclear power plants using mobile rescue robots: Emergency response to the fukushima nuclear accident using rescue robots," *J. Field Robot.*, vol. 30, no. 1, pp. 44–63, Jan. 2013, doi: [10.1002/rob.21439](https://doi.org/10.1002/rob.21439).
- [8] C. Assad, M. T. Wolf, J. Karras, J. Reid, and A. Stoica, "JPL BioSleeve for gesture-based control: Technology development and field trials," in *Proc. IEEE Int. Conf. Technol. Practical Robot Appl. (TePRA)*, May 2015, pp. 11–12.
- [9] J. Liu, X. Zhang, and G. Hao, "Survey on research and development of reconfigurable modular robots," *Adv. Mech. Eng.*, vol. 8, no. 8, pp. 1–21, Aug. 2016, doi: [10.1177/1687814016659597](https://doi.org/10.1177/1687814016659597).
- [10] R. Guzman, R. Navarro, J. Ferre, and M. Moreno, "Rescuer: Development of a modular chemical, biological, radiological, and nuclear robot for intervention, sampling, and situation awareness," *J. Field Robot.*, vol. 33, no. 7, pp. 931–945, 2016, doi: [10.1002/rob.21588](https://doi.org/10.1002/rob.21588).
- [11] E. Karamipour, S. F. Dehkordi, and M. H. Korayem, "Reconfigurable mobile robot with adjustable width and length: Conceptual design, motion equations and simulation," *J. Intell. Robotic Syst.*, vol. 99, nos. 3–4, pp. 797–814, Sep. 2020, doi: [10.1007/s10846-020-01163-7](https://doi.org/10.1007/s10846-020-01163-7).
- [12] Z. Jinzheng, J. Qichun, W. Qi, and Z. Peng, "Analysis and simulation of interaction mechanism between agricultural tracked vehicle and ground," in *Proc. Int. Conf. Comput. Syst., Electron. Control (ICCSEC)*, Dec. 2017, pp. 178–182, doi: [10.1109/ICCSEC.2017.8446867](https://doi.org/10.1109/ICCSEC.2017.8446867).
- [13] J. Y. Wong and W. Huang, "Approaches to improving the mobility of military tracked vehicles on soft terrain," *Int. J. Heavy Vehicle Syst.*, vol. 15, nos. 2–4, p. 127, 2008, doi: [10.1504/IJHVS.2008.022239](https://doi.org/10.1504/IJHVS.2008.022239).
- [14] C. B. Yang, L. Gu, and Q. Li, "Finite element simulation of track shoe and ground adhesion," *Appl. Mech. Mater.*, vols. 644–650, pp. 402–405, Sep. 2014, doi: [10.4028/www.scientific.net/AMM.644-650.402](https://doi.org/10.4028/www.scientific.net/AMM.644-650.402).
- [15] K. Nishiyama, H. Nakashima, H. Shimizu, J. Miyasaka, and K. Ohdoi, "2D FE-DEM analysis of contact stress and tractive performance of a tire driven on dry sand," *J. Terramech.*, vol. 74, pp. 25–33, Dec. 2017, doi: [10.1016/j.jterra.2017.09.003](https://doi.org/10.1016/j.jterra.2017.09.003).
- [16] G. Ishigami, A. Miwa, K. Nagatani, and K. Yoshida, "Terramechanics-based model for steering maneuver of planetary exploration rovers on loose soil," *J. Field Robot.*, vol. 24, no. 3, pp. 233–250, Mar. 2007, doi: [10.1002/rob.20187](https://doi.org/10.1002/rob.20187).
- [17] K. Amudha, K. V. Reshma, N. R. Ramesh, C. R. Deepak, G. A. Ramadass, and M. A. Atmanand, "Estimation of sinkage and breakout forces for tracked vehicle for soft soils," in *Proc. Oceans Taipei*, Apr. 2014, pp. 1–7, doi: [10.1109/OCEANS-TAIPEI.2014.6964444](https://doi.org/10.1109/OCEANS-TAIPEI.2014.6964444).
- [18] L. Li, W. Wang, D. Wu, and Z. Du, "Research on obstacle negotiation capability of tracked robot based on terramechanics," in *Proc. IEEE/ASME Int. Conf. Adv. Intell. Mechatronics*, Jul. 2014, pp. 1061–1066, doi: [10.1109/AIM.2014.6878221](https://doi.org/10.1109/AIM.2014.6878221).
- [19] J. Wachter, R. Mikut, and F. Buse, "Modeling and force control of a terramechanical wheel-soil contact for a robotic manipulator used in the planetary rover design process," in *Proc. IEEE/RSJ Int. Conf. Intell. Robots Syst. (IROS)*, Nov. 2019, pp. 560–565, doi: [10.1109/IROS40897.2019.8967900](https://doi.org/10.1109/IROS40897.2019.8967900).
- [20] J. Y. Wong, P. Jayakumar, E. Toma, and J. Preston-Thomas, "Comparison of simulation models NRRM and NTVPM for assessing military tracked vehicle cross-country performance," *J. Terramech.*, vol. 80, pp. 48–131, Dec. 2018, doi: [10.1016/j.jterra.2018.10.002](https://doi.org/10.1016/j.jterra.2018.10.002).
- [21] Y. Yang, Y. Sun, and S. Ma, "Effect of lug sinkage length to drawbar pull of a wheel with an actively actuated lug on sandy terrain," in *Proc. IEEE Int. Conf. Robot. Autom. (ICRA)*, May 2014, pp. 2932–2937, doi: [10.1109/ICRA.2014.6907281](https://doi.org/10.1109/ICRA.2014.6907281).
- [22] Y. Yang, Y. Sun, R. Yamamoto, and S. Ma, "Influence of moving direction on normal force acting on a single lug during translational motion in sandy soil," in *Proc. IEEE Int. Conf. Robot. Biomimetics (ROBIO)*, Dec. 2014, pp. 425–430, doi: [10.1109/ROBIO.2014.7090368](https://doi.org/10.1109/ROBIO.2014.7090368).
- [23] L. Ding, Z. Deng, H. Gao, J. Tao, K. D. Iagnemma, and G. Liu, "Interaction mechanics model for rigid driving wheels of planetary rovers moving on sandy terrain with consideration of multiple physical effects," *J. Field Robot.*, vol. 32, no. 6, pp. 827–859, Aug. 2014, doi: [10.1002/rob.21533](https://doi.org/10.1002/rob.21533).
- [24] Y. Ma, Q. Zhu, Q. Yan, H. Zheng, and A. Winfield, "Terramechanics-based modeling of locomotion characteristics of miniature tracked unmanned ground vehicle," in *Proc. Int. Conf. Modeling, Identificat. Control*, Jun. 2011, pp. 92–97, doi: [10.1109/ICMIC.2011.5973682](https://doi.org/10.1109/ICMIC.2011.5973682).
- [25] L. Ding, Z. Deng, H. Gao, J. Guo, D. Zhang, and K. D. Iagnemma, "Experimental study and analysis of the wheels' steering mechanics for planetary exploration wheeled mobile robots moving on deformable terrain," *Int. J. Robot. Res.*, vol. 32, no. 6, pp. 712–743, May 2013, doi: [10.1177/0278364912468357](https://doi.org/10.1177/0278364912468357).
- [26] L. Ding, L. Huang, S. Li, H. Gao, H. Deng, Y. Li, and G. Liu, "Definition and application of variable resistance coefficient for wheeled mobile robots on deformable terrain," *IEEE Trans. Robot.*, vol. 36, no. 3, pp. 894–909, Jun. 2020, doi: [10.1109/TRO.2020.2981822](https://doi.org/10.1109/TRO.2020.2981822).
- [27] J. Y. Wong, *Theory of Ground Vehicles*. New York, NY, USA: Wiley, 2008, pp. 82–106.
- [28] W. Wang, Z. Du, and L. Sun, "Dynamic load effect on tracked robot obstacle performance," in *Proc. IEEE Mechatronics Int. Conf.*, May 2007, pp. 1–6, doi: [10.1109/ICMECH.2007.4280041](https://doi.org/10.1109/ICMECH.2007.4280041).



YIDONG BAI was born in Handan, Hebei, China, in 1991. He received the M.S. degree in mechanical engineering from the Hebei University of Engineering, Hebei, in 2018. He is currently pursuing the Ph.D. degree in mechanical engineering with the School of Mechanical Engineering, Hebei University of Technology, Tianjin, China. His research interests include structural design of special robots especially around mobile robots, terramechanics, dynamic analysis, manufacturing, and mechatronics systems.



LINGYU SUN (Member, IEEE) received the M.S. and Ph.D. degrees from the Hebei University of Technology, in 2005 and 2009, respectively. He is currently an Associate Professor with the Hebei University of Technology. His main research interests include structural design of special robots especially around mobile robots and intelligent control technology of special robot.



MINGLU ZHANG (Member, IEEE) received the Ph.D. degree from Tianjin University, in 1997. He is currently a Professor with the School of Mechanical Engineering, Hebei University of Technology, Tianjin, China. He has authored over 150 articles in refereed journals and proceedings in the areas of mechanical engineering and intelligent robots. He is the Leader of the Innovation Team of Key Technologies of Robots in Service in Special Environments of the Ministry of Education of China. He has been presiding several National Key Research and Development Program and the key project of the National Natural Science Foundation of China. His research interests include mechanism design and control of special robots, deep learning, and computer vision.

• • •